# UC San Diego
## UC San Diego Previously Published Works

**Title**

Human Induced Pluripotent Stem Cell-Derived Macrophages Ameliorate Liver Fibrosis

**Permalink**

https://escholarship.org/uc/item/8jk531w2

**Journal**

Stem Cells, 39(12)

**ISSN**

1066-5099

**Authors**

Pouyanfard, Somayeh

Meshgin, Nairika

Cruz, Luisjesus S

et al.

**Publication Date**

2021-12-01

**DOI**

10.1002/stem.3449

Peer reviewed

REGENERATIVE MEDICINE

# Human Induced Pluripotent Stem Cell-Derived Macrophages Ameliorate Liver Fibrosis

Somayeh Pouyanfard[1] | Nairika Meshgin[2] | Luisjesus S Cruz[1] | Karin Diggle[2] | Hamidreza Hashemi[3] | Timothy V Pham[4] | Manuel Fierro[1] | Pablo Tamayo[4] | Andrea Fanjul[5] | Tatiana Kisseleva[2] | Dan S Kaufman[1]

[1]Department of Medicine, University of California, La Jolla, California, USA

[2]Department of Surgery, University of California San Diego, La Jolla, California, USA

[3]Immunity and Pathogenesis Program, Sanford Burnham Prebys Medical Discovery Institute, La Jolla, California

[4]Moores Cancer Center and Department of Medicine, University of California San Diego, La Jolla, California, USA

[5]Gastroenterology Drug Discovery Unit, Takeda Pharmaceutical Company Limited, San Diego, California, USA

**Correspondence**
Dan S. Kaufman; Department of Medicine, University of California, San Diego, La Jolla, California, USA; Phone number +1-858-822-1777;
Email: dskaufman@ucsd.edu

## ABSTRACT

With an increasing number of patients with degenerative hepatic diseases such as liver fibrosis, and a limited supply of donor organs, there is an unmet need for therapies that can repair or regenerate damaged liver tissue. Treatment with macrophages that are capable of phagocytosis and anti-inflammatory activities such as secretion of matrix metalloproteinases (MMPs) provide an attractive cellular therapy approach. Human induced pluripotent stem cells (iPSCs) are capable of efficiently generating a large-scale, homogenous population of human macrophages using fully defined feeder- and serum-free differentiation protocol. Human iPSC-macrophages exhibit classical surface cell markers and phagocytic activity similar to peripheral blood-derived macrophages. Moreover, gene and cytokine expression analysis reveal that these macrophages can be efficiently polarized to pro-inflammatory M1 or anti-inflammatory M2 phenotypes in presence of LPS + IFN-γ and IL-4 + IL-13, respectively. M1 macrophages express high level of CD80, TNF-α, and IL-6 while M2 macrophages show elevated expression of CD206, CCL17, and CCL22. Here, we demonstrate that treatment of liver fibrosis with both human iPSC-derived macrophage populations and especially M2 subtype significantly reduces fibrogenic gene expression and disease associated histological markers including Sirius Red, αSMA and Desmin in immunodeficient $Rag2^{-/-}\gamma c^{-/-}$ mice model, making this approach a promising cell-based avenue to ameliorate fibrosis.

### Significance Statement

Improved treatment for diseased or degenerated tissues and organs is greatly needed. These studies demonstrate the ability to efficiently derive macrophages from human iPSCs with the ability to improve liver fibrosis in a mouse xenograft model. This work enables clinical translation to use these iPSC-derived cells to better treat diverse fibrotic diseases.

## 1 | INTRODUCTION

Chronic toxic liver injury due to various etiologies including viral infection (hepatitis B and C), metabolic disorders (non-alcoholic steatohepatitis), exposure to chemicals (alcoholic liver diseases) or autoimmune diseases (autoimmune hepatitis) can lead to the development of liver fibrosis and cirrhosis (1). Liver injury leads to hepatocyte death, recruitment of inflammatory cells, and activation of myofibroblasts which secrete extracellular matrix (ECM) proteins and result in a fibrous scar. Liver fibrosis progresses to cirrhosis, hepatocellular carcinoma, and eventual liver failure (2) where organ transplantation is the only treatment option (3). An alternative therapy is

transplantation of cells that enable liver repair and/or regeneration. Transplantation of myeloid cells alone (4,5) or in combination with mesenchymal stem/stromal cells (MSCs) (6) have been shown to suppress inflammatory responses, and as a result, lead to the improvement of liver function. Infusion of autologous macrophages in patients with end stage liver disease (7) has also shown promise in clinic. Several other cell types have shown efficacy in preclinical models, including hepatocytes (8), liver sinusoidal endothelial cells (9), and endothelial progenitor cells (10).

Watanabe et al. (11) demonstrated that combination of MSCs and macrophages had a synergistic effect and reduced liver fibrosis and enhanced liver function in mice with carbon tetrachloride ($CCl_4$)-induced fibrosis. This synergistic effect was attributed to the fact that MSCs induced macrophage polarization towards an M2 phenotype with high phagocytic capacity and increased expression of MMPs. Host macrophages and neutrophils were also shown to infiltrate the fibrotic region after combination therapy and contributed to liver fibrosis regression and promoted regeneration along with transplanted cells.

Another study investigated the regenerative function of murine bone marrow-derived macrophages (BMM) in a $CCl_4$-induced mouse model of liver fibrosis. Although the macrophages were not polarized to either M1 or M2, they found that intraportal injection of BMM led to an up-regulation of chemokines (MCP-1, MIP-1a, MIP-2) followed by hepatic recruitment of endogenous macrophages and neutrophils that delivered MMPs-13 and -9, respectively, to the scar site. There was a reduction in the number of hepatic myofibroblasts, and increased expression of the anti-inflammatory and tissue regenerative factors [(IL-10, TWEAK (TNFSF12) and oncostatin M (OSM)]. These studies demonstrate clinically relevant improvement of liver fibrosis upon macrophage treatment (4).

Haideri et al. assessed the reparative function of murine embryonic stem cell (mESC)-derived macrophage in comparison to mouse BMM in a $CCl_4$-injury model. They found that mESC-derived macrophages were more skewed towards an anti-inflammatory phenotype, and therefore more able to reduce fibrosis compared to BMM. In these studies, mESC-derived macrophages reduced the amount of liver fibrosis to 50% of control treatment, decreased the number of fibrogenic myofibroblasts and activated liver progenitor cells (12).

Macrophages are of particular interest due to their intrinsic plasticity (13). While classically activated M1 macrophages are known to drive inflammation and activation of hepatic stellate cells (HSCs) and myofibroblasts, M2 macrophages are able to alleviate inflammation and stimulate regeneration in the injured liver (14). Therefore, macrophage polarization to an anti-inflammatory M2 phenotype provides a novel strategy for treatment of liver fibrosis of different etiologies.

To test this hypothesis, we developed a novel method to generate macrophages from human induced pluripotent stem cells (iPSCs) and differentiate them to the M1 or M2 phenotype. Furthermore, we tested the efficiency of human iPSC-derived macrophages to ameliorate liver fibrosis in an established immunodeficient $Rag2^{-/-}\gamma c^{-/-}$ mouse model of liver fibrosis. Although $Rag2^{-/-}\gamma c^{-/-}$ mice lack T and B cells, they retain the myeloid cell population, and develop significant liver fibrosis in response to $CCl_4$-induced toxic liver injury. Here, we report that administration of human iPSC-derived macrophages improved liver function, reduced inflammation and development of liver fibrosis, and improved hepatocyte function. Human iPSCs are able to generate sufficient numbers of human macrophages with an anti-inflammatory phenotype to provide a novel off-the-shelf cell-based therapy for liver diseases.

## 2 | RESULTS

### 2.1 | Efficient generation of human iPSC-derived macrophages

Here, we adapted a novel method to derive hematopoietic progenitor cells from human iPSCs for efficient production of human macrophages. A schematic representation of the macrophage production pipeline is depicted in Figure 1A and B. Briefly, human iPSCs expressing typical pluripotency markers (TRA-1-81$^+$ and SSEA-4$^+$; Figure 1 C) were aggregated in defined serum-free media supplemented with SCF, VEGF, BMP4 and Rock-Y to produce embryoid bodies (EBs), also considered hematopoietic organoids. After 6 days, the EBs in these conditions begin to generate hematopoietic and endothelial cells (CD34$^+$, CD31$^+$, CD43$^+$; Figure 1D) (15). The EBs were then transferred into flat bottom plates in macrophage differentiation media I containing M-CSF and IL-3. Under these conditions, EBs generate human macrophage progenitor cells (iPSC-MPro) that can then be supported to terminal differentiation towards human iPSC-M0 in macrophage differentiation media II containing M-CSF for 7 days. Human iPSC-M0 can then be polarized to human iPSC-M1 or human iPSC-M2 phenotypes in presence of LPS + IFN-γ or IL-4 + IL-13, respectively as described in detail below.

The EBs were able to continuously produce human iPSC-MPro for more than 12 weeks at a quantity of $5 \times 10^5$ to $1 \times 10^6$ cells/week/well in 6-well plate format (Figure 1E). These cells can be routinely harvested from suspension and further differentiated to human iPSC-M0 and subsequent human iPSC-M1 or human iPSC-M2 populations. Phenotypic characterization of human iPSC-MPro showed relatively uniform and consistent expression in most typical macrophage cell surface markers (CD14, CD11b, CD36, CD68 and SIRP-a) (Figure 1F).

### 2.2 | Human iPSC-derived macrophage populations show similar phenotypic characteristics to human peripheral blood-derived macrophages

To test whether human iPSC-MPro can be differentiated to human iPSC-M0 similar to human PB-M0, human iPSC-MPro and human PB-monocytes were terminally differentiated for 7 days in differentiation medium II and expression profile of a panel of typical macrophage cell surface markers were analyzed in human iPSC-M0 and human PB-M0 respectively (Figure 2A). The LPS receptor CD14, CD11b or

Macrophage-1 antigen (Mac-1), pan-macrophage marker CD68, costimulatory molecule CD86 (B7-2), MHC class II (HLA-DR) and signal regulatory protein α (SIRPα) which interacts with a broadly expressed transmembrane protein CD47, were all expressed at high levels in human iPSC-M0 and human PB-M0. Although phenotypic markers of human iPSC-MPro did not change upon differentiation to human iPSC-M0, gene ontogeny analysis revealed that some biological processes such as Fc receptor signaling, and phagocytosis were significantly up-regulated after differentiation to M0 while pathways involved in morphogenesis and development were enhanced in human iPSC-MPro population (Supplemental Figure 1A and B).

To assess whether human iPSC-derived macrophages resemble human PB-derived macrophages upon activation, cells were polarized to either M1 (in presence of IFN-γ and LPS) or M2 (in presence of IL-4 and IL-13) macrophages. Phenotype, gene expression, phagocytic activity and their ability to secrete cytokine/chemokine were evaluated. Flow cytometric analysis demonstrated that human iPSC-M1 and human PB-M1 exhibited similar expression of CD80; a classical M1 marker while M2 polarization resulted in more pronounced expression of mannose receptor CD206 (MRC1) in human iPSC-M2 compared to human PB-M2 (Figure 2B).

RT-qPCR analysis of M1 and M2-associated genes showed that pro-inflammatory phenotype markers CD80 and CD40 were upregulated in both human iPSC-M1 and human PB-M1. M2 culture conditions lead to increased expression of MRC1 and transglutaminase 2 (TGM2), with this expression notably higher in iPSC-M2 compared to PB-M2 (Figure 2C).

## 2.3 | Human iPSC-derived macrophage populations show similar functional characteristics to human peripheral blood-derived macrophages

Quantification of phagocytic capacity of 2 μm latex beads by different human iPSC and PB-derived macrophage populations demonstrated that while human iPSC-M1 and human PB-M1 had slightly lower phagocytic activity, human iPSC-M2 and human PB-M2 showed almost similar levels of phagocytosis compared to their M0 counterparts (Figure 2D-F). Overall, bead phagocytosis analysis demonstrates effective phagocytosis in all human iPSC and PB-derived macrophage populations.

We next evaluated cytokine expression profile of human iPSC-derived macrophages by MSD assay (Figure 2G). TNF-a and IL-6, two key pro-inflammatory cytokines together with IL-10 had remarkably high expression in the supernatants of human iPSC-M1 and only background level was detected in the supernatant of either human iPSC-M0 or human iPSC-M2. Corresponding upregulation of CCL17 (TARC) and CCL22 (MDC) was demonstrated in M2 activated macrophages. Taken together, the results demonstrate that human iPSC-derived macrophages share phenotypical and functional characterization to that of human PB-derived macrophages.

## 2.4 | RNA expression profile of human iPSC-M1 and human iPSC-M2 macrophage sub-types demonstrate distinct pro-inflammatory and anti-inflammatory phenotypes

Detailed characterization of more differentiated human iPSC-derived macrophage sub-types were assessed in RNA-seq analysis and compared with human PB counterparts. We had three aims: first, to assess the expression of known M1- and M2-specific markers in human iPSC and human PB-derived macrophages; second, to determine the expression of genes that are involved in liver fibrosis repair and regeneration; and third, to compare gene expression profile of human iPSC and human PB-derived macrophages.

Consistent with our RT-qPCR and MSD data, heatmap analysis of M1- and M2-associated genes demonstrated distinct expression profiles. CD80, CD40, TNF-a, IL-6 were upregulated in M1 and likewise CD206, TGM-2, CCL17 and CCL22 in M2 macrophages. Genes associated with inflammatory responses such as toll-like receptors (TLRs 1, 2, 7, 8) and inflammatory cytokines/chemokines [TNF-a, IL-6, IL-1b, IL-12, CCL2, CCL3 and TRAIL (TNFSF10)] were significantly upregulated in human iPSC-M1 compared to human iPSC-M2 macrophages. In contrast, anti-inflammatory markers such as CD9, IL-1RN, IL-27R, RCN1 (16-19) were only present in human iPSC-M2 subtype. Moreover, detailed characterization of human iPSC-M2 vs human iPSC-M1 sub-type, demonstrated elevated levels of scavenger receptors CD204 (SR-AI), CD206 (MRC1), CD209 (DC-SIGN) and Stabilin-1 (STAB-1) (20) in human iPSC-M2 (Figure 3A). A similar pattern was also observed in human PB-M1 and human PB-M2 subtypes (Supplemental Figure 2A). Interestingly, expression of several critical genes that are related to phagocytosis were differentially expressed in human iPSC-M1 and human iPSC-M2 sub-types. Specifically, MerTK, CD36, TREM-2 had higher expression in human iPSC-M2 while MARCO increased in human iPSC-M1. Similar pattern was observed for MMPs, while both groups shared almost similar expression of MMP-9 and 12, MMP-25 and MMP-7 were solely detected in human iPSC-M1 and human iPSC-M2, respectively (Figure 3B). Additionally, genes involved in tissue regeneration such as melanoma-associated transmembrane glycoprotein (Gpnmb) (21), Syndecan 1 (SDC-1) (22,23) were highly upregulated in human iPSC-M2 subtype. These data suggest that although both human iPSC-M1 and human iPSC-M2 subtypes share expression of some important genes involved in tissue repair and regeneration, human iPSC-M2 demonstrated more prominent expression of the related genes.

Moreover, gene ontogeny analysis of human iPSC and PB-derived macrophage populations demonstrated that human iPSC and human PB-derived M0, M1 and M2 largely shared transcriptomic profiles (86% between corresponding sub-types) while also revealing lineage-specific differentially expressed genes (Supplemental Figure 2B).

Although human iPSC-MPro were originally thought to be equivalent to human monocytes and show similar phenotypic expression to PB-monocyte (Supplemental Figure 3A), gene expression analysis supports that these two populations belong to a different cell ontogeny (Supplemental Figure 3B, C). Indeed, unlike human PB-monocytes

which arise from hematopoietic stem cells, human iPSC-MPro originate from yolk sac hematopoietic progenitor cells, self-renew during adult life through a Myb-independent proliferation mechanism and are more similar to tissue resident macrophages (12,24). In addition, hierarchical heatmap clustering of differentially expressed genes revealed close proximity of human iPSC-M2 and human iPSC-M0 and likewise in human PB-M2 and human PB-M0 macrophages (Supplemental Figure 3B, C), similar to other studies of ESC and iPSC-derived macrophages (12,25).

## 2.5 | CCl$_4$-injured mice Rag2$^{-/-}$γc$^{-/-}$ mice develop liver fibrosis

In a pilot study, to evaluate liver fibrosis in an immunodeficient Rag2$^{-/-}$γc$^{-/-}$ mice, fibrosis was induced by gradual increase of CCl$_4$ administration throughout the period of 8 weeks. In comparison with the control mice that received corn oil alone, CCl$_4$ -injured Rag2$^{-/-}$γc$^{-/-}$ mice developed bridging fibrosis, shown by increased area of Sirius Red staining (4-fold), and activation of aSMA$^+$ and Desmin$^+$ aHSCs/myofibroblasts (Supplemental Figure 4A). Development of liver fibrosis in CCl$_4$-injured Rag2$^{-/-}$γc$^{-/-}$ mice was associated with the increased recruitment and activation of F4/80$^+$ macrophages, and increased expression of the fibrogenic genes Col1a1, αSMA, TIMP1, and LoxL2 in total tissue mRNA (Supplemental Figure 4B).

Evaluation of fibrosis regression (9 days after cessation of CCl$_4$) showed suppression in inflammatory responses and downregulation of ECM producing myofibroblasts, shown by decreased Sirius Red and aSMA histology, as well as reduced expression of fibrogenic genes (Supplemental Figure 4). Based upon these data, a therapeutic regimen of human iPSC administration into the immunodeficient CCl$_4$-injured Rag2$^{-/-}$γc$^{-/-}$ mice was adopted for our follow up experiments to recapitulate treatment of patients with liver fibrosis where the etiological agent remains present.

## 2.6 | Administration of human iPSC-derived macrophages ameliorates liver fibrosis in Rag2$^{-/-}$γc$^{-/-}$ mice

To determine the therapeutic effect of human iPSC-derived macrophages on liver fibrosis in CCl$_4$-injured Rag2$^{-/-}$γc$^{-/-}$ mice, human iPSC-M1 or -M2 (5 x 10$^6$ cells/mouse, 2 x IP injection) were therapeutically administered during the CCl$_4$ regimen into Rag2$^{-/-}$γc$^{-/-}$ mice that already developed liver fibrosis, with a 1-week interval between doses (Figure 4A). Control mice were given corn oil only. Mice were sacrificed one week after the second and final iPSC-M1 or -M2 injection. Liver tissue and serum were collected and analyzed (Figure 4A-D).

The liver weight to body weight ratio was significantly lower in human iPSC-M2 treated Rag2$^{-/-}$γc$^{-/-}$ mice compared to both CCl$_4$-injured or CCl$_4$-injured, iPSC-M1 treated mice (P < 0.01) (Figure 4B)

and was associated with the improvement of liver gross morphology (Figure 4C). Quantification of Sirius Red staining revealed a significant decrease of collagen deposition in CCl$_4$-injured Rag2$^{-/-}$γc$^{-/-}$ mice administered with human iPSC-M2 (2.0% total positive area) compared to CCl$_4$ treatment alone (4.1%, P < 0.001) as well as compared to iPSC-M1 treated mice (3.4%, P < 0.001). Interestingly, mice treated with human iPSC-M1 also showed a significant reduction in fibrosis compared to CCl$_4$ treated mice, despite the pro-inflammatory profile of these cells *ex-vivo* (P = 0.003).

Expression of αSMA was significantly decreased in Rag2$^{-/-}$γc$^{-/-}$ mice administered with human iPSC-M2 (9.5%) treated groups compared to CCl$_4$ treatment alone (13.0%, P < 0.0001) (Figure 4D). Hepatic stellate cells (HSCs) are known to activate and deposit extracellular matrix proteins in response to injury (26). In conjunction, staining for desmin$^+$ activated HSCs was significantly reduced in human iPSC-M1 (9.6%) and -M2 (9.3%) treated groups compared to CCl$_4$ treatment alone (11.4%) (P < 0.0001). Staining for F4/80$^+$ inflammatory macrophages was significantly reduced in human iPSC-M1 (9.9%) and human iPSC-M2 (9.0%) treated groups compared to CCl$_4$ treatment alone (11.3%) (P = 0.03, 0.0002, respectively) (Figure 4D). Quantification of staining for histology is shown (Figure 4D).

Together, these data revealed that therapeutic administration of both human iPSC-M1 and -M2 cells *in vivo* results in reduced fibrosis and inflammation. While iPSC-M2 demonstrated stronger downregulation of clinically relevant fibrotic markers, we unexpectedly also observed profound antifibrogenic potential in iPSC-M1. Resolution of fibrosis in the presence of iPSC-M1 may be indicative of a shift in phenotype upon injection to the peritoneal cavity of Rag2$^{-/-}$γc$^{-/-}$ mice, though the mechanism of this shift is unknown. Ma et al. (27) report on the therapeutic potential of M1 polarized BMDMs to ameliorate fibrosis via the recruitment of endogenous macrophages and NK cells that promote HSC apoptosis through MMPs and TRAIL (27). While Rag2$^{-/-}$γc$^{-/-}$ mice lack NK cells, iPSC-M1 cells can potentially recruit MMP secreting-endogenous macrophages with powerful antifibrotic effects during injury.

## 2.7 | Gene expression profiles are less inflammatory in human iPSC-derived macrophage-treated mice

Expression of fibrogenic markers was evaluated by RT-qPCR (Figure 5A). Collagen1a1 (Col1a1) and αSMA, ECM protein components of fibrotic scars deposited by activated HSCs during injury to the liver, were significantly reduced in iPSC-M1 and -M2 treated mice compared to CCl$_4$ only (P = 0.001, 0.008 for Col1a1 in iPSC-M1 and -M2, respectively; P = 0.0003, 0.007 for αSMA in iPSC-M1 and -M2, respectively). LoxL2, a fibrosis-associated enzyme responsible for crosslinking connective tissues in scar formation, was significantly lower in both iPSC-M1 and -M2 treated mice (P = 0.004 and P = 0.009, respectively). TGF-β1 was also significantly downregulated in both iPSC-M1 and −2 treated mice (P = 0.01). TIMP-1 showed a non-significant decrease in the liver of fibrotic mice after both iPSC-

M1 or -M2 administration, with markedly lower levels in the human iPSC-M2 group. Notably, there was no significant differences in gene expression profiles between iPSC-M1 and -M2 treated animals.

## 2.8 | Cytokine profile in livers of mice treated with human iPSC-derived macrophages is less fibrogenic/inflammatory

Cytokine expression profile of total tissue homogenate was analyzed by luminex assay (Figure 5B). Analysis of several pro-inflammatory cytokines/chemokines including MCP1, VCAM-1 and MIP-1β showed a slightly reduced non-significant trend in human iPSC-M2 treated animals compared to CCl$_4$ treatment alone. While the level of TGF-β and IFN-β in liver decreased slightly in both human iPSC-M1 and iPSC-M2 groups, MIP-1γ only showed a significant decrease in iPSC-M1 group. Consistent with the trend we observed in total tissue gene expression analysis, TIMP-1 expression decreased more noticeably in the iPSC-M2 treated group compared to CCl$_4$ treatment alone. Levels of IL-17A and IL-27, two cytokines that are reported to have a collaborative role in liver regeneration (28) were elevated in liver of mice treated with human iPSC-M2 compared to CCl$_4$ treatment alone.

Interestingly, in corroboration with our other *in vivo* findings, there were no significant differences between cytokine profiles in iPSC-M1 and -M2 treated livers. This similarity is surprising due to the dramatic, classic pro-inflammatory profile of human iPSC-M1 and anti- inflammatory profile of human iPSC-M2 *ex vivo* (Figure 3). Because these data shows that our macrophages were indeed polarized to M1 and M2 phenotypes, we expected fibrosis to be exacerbated by iPSC-M1. Conversely, iPSC-M1 and -M2 had a comparable therapeutic effect on fibrosis and followed the same trends in cytokine expression, suggesting that either M undergo a shift to an anti-inflammatory phenotype when injected into mice or both iPSC-M1 and iPSC-M2 populations contributed to fibrosis resolution.

Overall, these data support the hypothesis that administration of human iPSC-derived macrophages, ameliorate liver fibrosis possibly by decreasing pro-inflammatory cytokines in the liver microenvironment, thus improving liver function and regeneration.

## 2.9 | Human iPSC-derived macrophages do not mainly localize into liver tissue after intraperitoneal administration

In a pilot study, 3 x 10$^6$ PKH-26-labeled human iPSC-M0 macrophages were injected IP in uninjured mice and tracked over 16 days using UV microscopy. Cells remained primarily in the peritoneal cavity and only few cells were detected in the capsules of the liver (Supplemental Figure 5A), spleen, pancreas, and kidneys (not shown).

In a follow up study, 20 x 10$^6$ TdTomato-expressing human iPSC-M2 macrophages were injected IP during the course of CCl$_4$ induced injury. The goals were to track whether macrophages migrate to the liver, and to evaluate whether a larger dose of human iPSC-M2

macrophages would have a more profound impact on fibrosis reduction. Staining with human CD68 antigen (a marker of myeloid cells) on liver tissue showed that human iPSC macrophages could not be detected after IP administration into either uninjured or CCl$_4$-injured mice treated with 1 dose of 20 x 10$^6$ human iPSC-M2 macrophages (Supplemental Figure 5B). Although we did not observe homing to the liver by iPSC-M2 macrophages, they produced a notable therapeutic effect on liver injury (Supplemental Figure 5C). Cells introduced via IP injection may transiently pass through the liver resulting in changes in the microenvironment and production of anti-inflammatory factors with more persistent impacts. Alternatively, injected iPSC macrophages may secrete cytokines directly into the peritoneal cavity, leading to absorption of these anti-inflammatory factors by peritoneal vasculature into portal tract (29).

Consistent with our previous findings, administration of an increased dose of human iPSC-M2 macrophages (20 x 10$^6$), resulted in significant reduction in fibrosis (Supplemental Figure 5C). Collagen deposition, shown by Sirius Red staining, was significantly reduced in human iPSC-M2 macrophage injected mice compared with CCl$_4$ treated mice ($P = 0.01$). aSMA staining was also significantly reduced in mice treated with 20 x 10$^6$ human iPSC-M2 macrophages compared with mice given CCl$_4$ only ($P = 0.02$). Notably, injection of 20 x 10$^6$ human iPSC-M2 macrophages into either uninjured or CCl$_4$-injured mice did not result in any notable toxicity, suggesting that administration of human iPSC-derived macrophages is safe and tolerable. These data confirmed our initial results that administration of human iPSC-derived macrophages, have a significant impact on ameliorating fibrosis, further highlighting the potential of human iPSC-derived macrophages as an anti-fibrotic liver therapy.

## 3 | DISCUSSION

The present study provides evidence that human iPSC-derived macrophages, especially human iPSC-M2, improve liver fibrosis and stimulate regeneration in CCl$_4$- injured mice. To our knowledge, our study is the first to evaluate the administration of human iPSC-derived macrophages in an immunodeficient mouse model of liver injury, although other studies have investigated the effect of mouse BM- and ESC-derived macrophages (4,12). Moreover, the mouse BM-M2 population has also been shown to play a crucial reparative role in cardiac infarction (30).

We have utilized an efficient method using fully defined feeder- and serum-free differentiation protocol for rapid generation of large numbers of human iPSC-derived macrophages which exhibited characteristic macrophage morphology and expressed macrophage specific cell surface antigens. This methodology provides a critical step towards obtaining clinical scale production of human iPSC-derived macrophages for cell therapy approaches, including liver fibrosis treatment. Although other protocols for differentiation of human ESCs and iPSCs to macrophages have been utilized to study the effect of macrophage in disease modeling, such as studies to model COVID-19 (31,32).

Macrophages play an important role in regulating inflammatory responses, so we tested these human iPSC-M1 and M2 polarized macrophages in a mouse model of $CCl_4$-induced liver fibrosis. We have demonstrated that both human iPSC-macrophage populations including iPSC-M1 and iPSC-M2 resulted in fibrosis attenuation/regression in the $CCl_4$ model of liver fibrosis. In both groups, clinical markers of fibrosis were significantly reduced as indicated by staining of Sirius Red, aSMA and desmin. Of note, the clinically relevant fibrosis marker Sirius Red, a marker of collagen deposition, demonstrated a more significant and remarkable reduction after iPSC-M2 injection.

Several potential mechanisms mediate fibrosis regression and contribute to the regenerative responses including the activation of collagenase- and MMP- secreting macrophages in parallel with decreased activity of TIMPs (33-36). Notably, we observed significant expression of MMP-2, 7, 15 and 19, and reduced levels of TIMP-1 in human iPSC-M2 macrophages, which could explain why collagen deposition was more significantly reduced in iPSC-M2-treated mice compared to iPSC-M1. Macrophages also act as professional phagocytes with the capacity to engulf cellular debris and apoptotic cells, and they play a critical role in the resorption of fibrous scar (37,38). Our human iPSC-M2 macrophages expressed high levels of surface receptors MerTK, CD36, TREM-2 which have previously reported to promote tissue repair (39-41), as well as genes that are involved in tissue regeneration such as Gpnmb (21) and SDC-1 (22,23).

However, we also observed a strong therapeutic effect in human iPSC-M1 injected mice, which we attribute to expression of several members of the MMP family, phagocytosis receptor MARCO, and anti-inflammatory cytokine IL-10 (Figure 2G). While the anti-inflammatory cytokine IL-10 was expected to be upregulated upon M2 activation, we observed high levels of IL-10 in M1 supernatant and low expression in M2 supernatant. According to previous studies (42,43), secretion of IL-10 is thought to be one of the several feedback mechanisms after M1 polarization to limit excessive inflammatory responses. In fact, a more recent study from Ma et al. demonstrated the beneficial effects of adoptively transferred BM-M1 on liver scarring and regeneration in a mouse model of liver fibrosis (27). They reported that BM-M1 exhibit anti-fibrotic activity via recruitment of endogenous macrophages expressing MMP-2, 9, 13, increasing collagen degradation and hepatic growth factor (HGF) secretion, and inducing hepatocyte proliferation. They also found that NK cells migrated to the scar tissue leading to TRAIL-mediated apoptosis of HSCs and hampered fibrogenesis (27). Interestingly, in our study, TRAIL expression was significantly higher in human iPSC-M1 macrophages compared to human iPSC-M2 macrophages.

Several clinical studies have tested the impact of macrophages on human patients with severe liver disease (44). One such study from Forbes et al. on patients with cirrhosis tested the efficacy and safety of autologous macrophage therapy (7). They showed several non-invasive measures of fibrosis improved following macrophage infusion, including transient elastography, serum enhanced liver fibrosis (ELF) score, and collagen turnover markers PRO-C3 and C3M; in conjunction, patients had a decreased model end stage liver disease (MELD) score one year after the trial. Since this study used autologous

macrophages derived from an inflammatory, cirrhotic environment, a pro-inflammatory M1 polarized phenotype is assumed, yet antifibrotic therapeutic potential was achieved.

Taken together, both human iPSC-M1 and iPSC-M2 macrophages demonstrate signatures that contribute to the regenerative responses, including expression of collagenases and MMPs, and expression of phagocytic receptors and genes involved in anti-inflammatory activities including tissue repair and regeneration.

Since we used an immunodeficient mouse model, the effect of endogenous immune cells, especially macrophages and neutrophils, is less clear. Therefore, in order to mimic a more physiological liver microenvironment, we believe that administration of human macrophages in a humanized mouse model of liver injury would provide a better approach for future studies to better define these mechanisms involved in the resolution of liver fibrosis.

We were also interested in investigating the survival and homing of human iPSC-derived macrophages to different organs including the liver. Previously, Haideri et al. (12) found that mESC-derived macrophages repopulated the Kupffer cell compartment of clodronate-treated mice more efficiently than BM-derived macrophages. This is of particular importance because recent studies have indicated that the human iPSC-derived macrophage phenotype is more comparable to tissue-resident (rather than monocyte-derived) macrophages (24,45). In our study, we could not detect true human iPSC-macrophages localized in the liver. This could be due to the intraperitoneal route of injection we used vs the intravenous route utilized by Haideri et al (12) or cells might transiently pass through the liver compartment via peritoneal vasculatures. For future studies, injecting larger cell numbers intravenously and evaluating the homing of cells with a more fine-tuned strategy—such as monitoring for a shorter time after injection, utilizing intravital confocal microscopy detection, or primary cell isolation/characterization— will enable us to evaluate the homing of human iPSC macrophages.

Despite the use of PB-derived macrophages in several clinical studies, their broader application is restricted by limited cell number per donor, donor-to-donor variation and being less amenable to genetic engineering. The use of a homogenous, standardized, and off-the-shelf product such as human iPSC-derived macrophages provides a potentially superior approach for treatment of hepatic diseases where liver transplantation is the only therapeutic option. Our study provides an efficient system for rapid generation of homogenous macrophage populations with anti-fibrotic effects from human iPSCs, a key step towards normalizing the use of these cells as a clinical therapeutic for human diseases including chronic liver diseases.

## 4 | METHODS

### 4.1 | Induced pluripotent stem cells culture and macrophage differentiation

Human iPSCs derived from umbilical cord blood CD34^{+} cells (15,46-48) were maintained as undifferentiated cells on matrigel-

coated tissue culture flasks in mTeSR media (STEMCELL Technologies). Human iPSC-derived macrophages were generated according to previously described protocol (49) with some modifications. Briefly, 8000 human iPSCs were single cell passaged and then aggregated into spin embryoid bodies (EBs) by centrifugation on ultra-low attachment 96-well u-bottom plates (Corning) with cytokines that are essential for hematopoietic progenitor development (APEL media containing 40 ng/mL SCF, 20 ng/mL VEGF, 20 ng/mL BMP4 and 10 μM Rock-Y). EBs were then manually transferred (20 EBs per well) onto 0.1% gelatin-coated 6-well plates containing differentiation medium I (X-VIVO15 media (Lonza) supplemented with 1% penicillin-streptomycin (Gibco), 1% GlutaMAX (Gibco), 55 mM 2-Mercapnoethanol (Gibco), 50 ng/mL M-CSF and 25 ng/mL IL-3 (all from Peprotech)). Human iPSC-derived macrophage progenitor cells (iPSC-MPro) started to generate after 1-2 weeks. These cells were then collected and further differentiated to mature macrophages (human iPSC-derived macrophages) in differentiation medium II (X-VIVO15 media supplemented with 1% penicillin-streptomycin, 1% GlutaMAX and 100 ng/mL M-CSF) for 7 days.

## 4.2 | Isolation of peripheral blood monocyte and differentiation to macrophage

Adult human blood was obtained from anonymous donors through the San Diego Blood Bank. Peripheral blood mononuclear cells (PBMC) were isolated by Ficoll-Paque Plus (GE Healthcare) density-gradient centrifugation from heparinized buffy coats. Monocytes (PB-monocyte) were isolated by CD14 positive selection using anti-CD14 magnetic beads (Miltenyi Biotec) according to manufacturer's instructions and then further differentiated to macrophages (PB-macrophages) in differentiation medium II for 7 days.

## 4.3 | Macrophage polarization

Human iPSC-MPro or PB-monocytes were cultured in differentiation medium II for 7 days to differentiate to M0 (iPSC-M0 and PB-M0). M0 macrophages were then polarized to either M1 (iPSC-M1 and PB-M1) or M2 (iPSC-M2 and PB-M2) macrophages for 48 hours in differentiation medium II supplemented with different stimuli: 100 ng/mL LPS (Sigma) and 20 ng/mL IFN-g (R&D) for M1 polarization or 20 ng/mL IL-4 and 20 ng/mL IL-13 (R&D) for M2 polarization. The effect of activation was evaluated by quantifying changes in different phenotypic markers by flow cytometry, quantitative RT-PCR and RNA sequencing.

## 4.4 | Flow cytometry

Single-cell suspensions were stained with antibodies listed in Table 1. Flow cytometry was performed on a BD LSR II or Acea Novocyte 3000, and the data were analyzed using Flowjo or NovoExpress software (Acea Biosciences).

## 4.5 | Quantitative real-time PCR (qRT-PCR)

Total RNA was extracted from human iPSC and PB-derived macrophage populations using RNeasy Mini Kit (Qiagen) according to manufacturer's instructions. Complementary DNA (cDNA) was synthesized using iScript gDNA Clear cDNA Synthesis Kit (Bio-Rad) according to manufacturer's instruction. qRT-PCR was performed using the CFX384 Touch Real-Time PCR Detection System (Bio-Rad) and analyzed with CFX Manager Software (Bio-Rad). The TaqMan Gene Expression Assays (ThermoFisher Scientific) was used to detect gene expression. The $\Delta\Delta$Ct method was used with GAPDH to normalize cDNA levels and the "control" sample of each experiment was used as a calibrator to calculate relative change in gene expression. All data are presented as fold-change over the expression level of the calibrator.

## 4.6 | RNA-Seq and analysis

All RNA sequencing analysis was performed by Novogene Corporation Inc. (Sacramento, CA, USA). All experiments were performed as 3 biological replicates. Differential expression analysis of two conditions/groups was done by using the DESeq2 R package, while the significant criterion was padj<0.05.

## 4.7 | Cytospin and Giemsa staining

Cell suspension ($10^5$) of different macrophage populations were loaded on slides using Cytospin (Thermo Shandon, Basingstoke, Hampshire, UK), spun at 500 rpm for 5 min and air-dried. Dried slides were stained with modified Giemsa (Polysciences, Inc.), according to manufacturer's instruction. Slides were mounted with round coverslips using Permount Mounting Medium (Fisher Chemical) and dried overnight. Images were taken using EVOS FLc (Life Technologies).

## 4.8 | Bead phagocytosis assay

For analysis of phagocytosis, different macrophage populations were incubated with carboxylate-modified red fluorescent latex beads with a mean diameter of 2 μm (L3030; Sigma-Aldrich) at a ratio of 1:10 for 2 hours. After repeated washing, the cells were analyzed by flow cytometry.

## 4.9 | Latex bead imaging

About $1.0 \times 10^6$ macrophages were stained following CellTrace Violet Proliferation Kit (Invitrogen) protocol for suspension cells. Stained cells were then seeded on microscope cover glass (Fisherbrand) in 24-well plates coated with 0.1% gelatin and cultured overnight in differentiation medium II to allow re-attachment. On the following day, cells were incubated with latex beads as mentioned above. Cells were then fixed using 4% paraformaldehyde for 15 minutes at room temperature and washed with DPBS twice. Microscope cover glass was then mounted on glass slides using Permount Mounting Medium (Fisher Chemical) and dried overnight. Images were taken using EVOS FLc (Life Technologies).

## 4.10 | Cytokine/chemokine measurement

Supernatants from activated macrophage cultures were collected after 48 hours and frozen at $-80^\circ$C until assayed. Concentration of cytokines and chemokines were measured by Meso Scale Discovery (MSD), according to manufacturer's instructions.

## 4.11 | Animal model of liver fibrosis

Eight- to ten-week-old Rag2$^{-/-}$γc$^{-/-}$ mice (equal ratio of male and female) were purchased from the Jackson Laboratories and kept at the animal facility at the University of California, San Diego in accordance with IACUC regulations. Mice were divided into 4 groups (corn oil: 9, CCl$_4$: 14, human iPSC-M1 and iPSC-M2:13 mice) and given increasing doses of CCl$_4$ in corn oil (50), or corn oil only as a control, over the course of 8 weeks. Doses of CCl$_4$ were slowly increased from 1:16 to 1:8 to 1:4. CCl$_4$ was administered via oral gavage twice weekly over this 8-week regimen. A timeline of the *in vivo* process is shown in Figure 4A.

Groups of mice were therapeutically treated with either human iPSC-M1 or iPSC-M2 ($5 \times 10^6$, intraperitoneal injection) during the last 2 weeks (weeks 6 and 7) of the CCl$_4$ regimen. Injections were given 1 week apart, and mice were sacrificed 1 week after the second injection.

## 4.12 | Histology

Formalin-fixed, paraffin embedded murine livers were stained with H&E, Sirius Red, anti-αSMA (ab5694; Abcam), anti-desmin (Rb-9014-P0; Thermo Fisher Scientific), anti-F4/80 (14-4801-82; Thermo Fisher Scientific) and anti-CD68 (ab955, Abcam) antibodies. HRP conjugated secondary antibodies were utilized (anti-rabbit MP-7401 and anti-rat MP-7444; Vector Laboratories). For CD68, a mouse- on-mouse staining kit was used to block nonspecific host antibody-antigen interactions (Vector Laboratories, PK-2200). Signals were

developed using DAB substrate (Vector Laboratories). Quantification of histological staining was done using ImageJ software.

## 4.13 | Quantitative real-time PCR (qRT-PCR) for fibrosis assessment

Quantitative RT-PCR was performed using QuantStudio 3 system (Applied Biosystems). Total RNA was isolated from mouse livers using PureLink RNA Mini kit (Invitrogen). Expression levels of selected genes were measured. The data are shown as fold change of mRNA level expression compared to control (mean ± SEM).

## 4.14 | Multiplex cytokine analysis on tissue homogenate

Levels of selected cytokines in liver homogenate were measured by the Rodent MAP 4.0-Mouse Sample Testing service provided by Ampersand Biosciences. Snap frozen total liver tissues were provided for analyses (https://www.ampersandbio.com/, Lake Clear, New York).

## 4.15 | Human iPSC-derived macrophage survival and homing

To monitor the localization of human iPSC-derived macrophages, $3 \times 10^6$ iPSC-M0 were labeled with PKH-26 red fluorescent dye (Sigma-Aldrich) and injected IP into eight-to ten-week-old uninjured Rag2$^{-/-}$γc$^{-/-}$ mice (51). Mice were harvested at various time points over the course of 16 days (3, 5, 7, 10, 12, 14, 16 days post macrophage injection). Harvested organs including liver, kidney, and spleen, and peritoneal lavage were examined under an Olympus UV microscope (Supplemental Figure 5A).

To monitor the homing of human iPSC-macrophages into the livers of CCl$_4$-injured Rag2$^{-/-}$γc$^{-/-}$ mice, a piggyBac plasmid expressing tdTomato (Vector Builder) was utilized to transfect human iPSCs using Amaxa Human Stem Cell Nucleofector Kit 1 (Lonza) following manufacturer's protocols. Transfected cells were cultured in presence of Puromycin (0.5 μg/mL) for 9 days until all cells expressed tdTomato and then they used to generate human iPSC-M2 macrophages as described above. $20 \times 10^6$ human iPSC-M2 were injected IP during week 7 of the CCl$_4$ regimen into Rag2$^{-/-}$γc$^{-/-}$ mice. One week later, livers were harvested and evaluated for the presence of tdTomato-expressing human iPSC-M2 via histology.

## 4.16 | Statistics

Statistical analysis was performed in GraphPad Prism 6.0 (GraphPad). Data are presented as the mean $-$/+ SE of the mean (SEM). Each figure legend denotes the statistical test used. ANOVA multiple

comparison P values were generated using Tukey's multiple comparisons test. For all figures, * indicates $P < 0.05$, ** indicates $P < 0.01$, *** indicates $P < 0.001$ and **** indicates $P < 0.0001$.

## 4.17 | Study approval

The studies were approved by the UCSD Institutional Animal Care and Use Committee and followed the NIH guidelines outlined in *Guide for the Care and Use of Laboratory Animals* (National Academies Press, 2011).

## DISCLOSURE OF POTENTIAL CONFLICTS OF INTEREST

DSK is a co-founder and advisor to Shoreline Biosciences and has an equity interest in the company. DSK also consults for Qihan Biotech and VisiCELL Medical for which he receives income and/or equity. Studies in this work are not related to work of those companies. The terms of these arrangements have been reviewed and approved by the University of California, San Diego in accordance with its conflict of interest policies.

## AUTHOR CONTRIBUTION

Design and implementation of studies, acquisition and analysis of data, writing and revision of manuscript: S.P.; implementation of studies, acquisition and analysis of data and review of manuscript: N.M.; implementation of studies, acquisition of data and review of manuscript: L.S.C.; acquisition of data: K.D.; analysis of data: H.H., T.V.P.; implementation of studies: M.F.; design of studies and analysis of data: P.T. and A.F.; design of studies, analysis of data, review and revision of manuscript: T.K. and D.S.K.

## DATA AVAILABILITY STATEMENT

The data that support the findings of this study are available from the corresponding author upon reasonable request.

## ORCID

*Dan S Kaufman* https://orcid.org/0000-0002-2003-2494

## REFERENCES

1. Wang P, Koyama Y, Liu X, et al. Promising Therapy Candidates for Liver Fibrosis. *Front Physiol*. 2016;7:47.
2. Kisseleva T, Brenner DA. The phenotypic fate and functional role for bone marrow-derived stem cells in liver fibrosis. *J Hepatol*. 2012;56(4):965-972.
3. Sze YK, Dhawan A, Taylor RM, et al. Pediatric liver transplantation for metabolic liver disease: experience at King's College Hospital. *Transplantation*. 2009;87(1):87-93.
4. Thomas JA, Pope C, Wojtacha D, et al. Macrophage therapy for murine liver fibrosis recruits host effector cells improving fibrosis, regeneration, and function. *Hepatology*. 2011;53(6):2003-2015.
5. Starkey Lewis P, Campana L, Aleksieva N, et al. Alternatively activated macrophages promote resolution of necrosis following acute liver injury. *J Hepatol*. 2020;73(2):349-360.
6. Mohamadnejad M, Alimoghaddam K, Bagheri M, et al. Randomized placebo-controlled trial of mesenchymal stem cell transplantation in decompensated cirrhosis. *Liver Int*. 2013;33(10):1490-1496.
7. Moroni F, Dwyer BJ, Graham C, et al. Safety profile of autologous macrophage therapy for liver cirrhosis. *Nat Med*. 2019;25(10):1560-1565.
8. Park S, In Hwang S, Kim J, et al. The therapeutic potential of induced hepatocyte-like cells generated by direct reprogramming on hepatic fibrosis. *Stem Cell Res Ther*. 2019;10(1):21.
9. Ding BS, Cao Z, Lis R, et al. Divergent angiocrine signals from vascular niche balance liver regeneration and fibrosis. *Nature*. 2014;505(7481):97-102.
10. Nakamura T, Torimura T, Sakamoto M, et al. Significance and therapeutic potential of endothelial progenitor cell transplantation in a cirrhotic liver rat model. *Gastroenterology*. 2007;133(1):91-107.e1.
11. Watanabe Y, Tsuchiya A, Seino S, et al. Mesenchymal Stem Cells and Induced Bone Marrow-Derived Macrophages Synergistically Improve Liver Fibrosis in Mice. *Stem Cells Translational Medicine*. 2019;8(3):271-284.
12. Haideri SS, McKinnon AC, Taylor AH, et al. Injection of embryonic stem cell derived macrophages ameliorates fibrosis in a murine model of liver injury. *NPJ Regen Med*. 2017;2:14.
13. Sica A, Mantovani A. Macrophage plasticity and polarization: in vivo veritas. *J Clin Invest*. 2012;122(3):787-795.
14. Duffield JS, Forbes SJ, Constandinou CM, et al. Selective depletion of macrophages reveals distinct, opposing roles during liver injury and repair. *J Clin Invest*. 2005;115(1):56-65.
15. Knorr DA, Ni Z, Hermanson D, et al. Clinical-scale derivation of natural killer cells from human pluripotent stem cells for cancer therapy. *Stem Cells Translational Medicine*. 2013;2(4):274-283.
16. Suzuki M, Tachibana I, Takeda Y, et al. Tetraspanin CD9 negatively regulates lipopolysaccharide-induced macrophage activation and lung inflammation. *J Immunol*. 2009;182(10):6485-6493.
17. Gabay C, Palmer G. Mutations in the IL1RN locus lead to autoinflammation. *Nat Rev Rheumatol*. 2009;5(9):480-482.
18. Peshkova IO, Fatkhullina AR, Mikulski Z, Ley K, Koltsova EK. IL-27R signaling controls myeloid cells accumulation and antigen-presentation in atherosclerosis. *Sci Rep*. 2017;7(1):2255.
19. Junkins RD, MacNeil AJ, Wu Z, McCormick C, Lin TJ. Regulator of calcineurin 1 suppresses inflammation during respiratory tract infections. *J Immunol*. 2013;190(10):5178-5186.
20. PrabhuDas MR, Baldwin CL, Bollyky PL, et al. A Consensus Definitive Classification of Scavenger Receptors and Their Roles in Health and Disease. *J Immunol*. 2017;198(10):3775-3789.
21. Li B, Castano AP, Hudson TE, et al. The melanoma-associated transmembrane glycoprotein Gpnmb controls trafficking of cellular debris for degradation and is essential for tissue repair. *FASEB J*. 2010;24(12):4767-4781.
22. Chung H, Multhaupt HA, Oh ES, Couchman JR. Minireview: Syndecans and their crucial roles during tissue regeneration. *FEBS Lett*. 2016;590(15):2408-2417.
23. Alexopoulou AN, Multhaupt HA, Couchman JR. Syndecans in wound healing, inflammation and vascular biology. *Int J Biochem Cell Biol*. 2007;39(3):505-528.
24. Buchrieser J, James W, Moore MD. Human Induced Pluripotent Stem Cell-Derived Macrophages Share Ontogeny with MYB-Independent Tissue-Resident Macrophages. *Stem Cell Reports*. 2017;8(2):334-345.
25. Zhang H, Xue C, Shah R, et al. Functional analysis and transcriptomic profiling of iPSC-derived macrophages and their application in modeling Mendelian disease. *Circ Res*. 2015;117(1):17-28.

26. Kisseleva T, Brenner DA. Role of hepatic stellate cells in fibrogenesis and the reversal of fibrosis. *J Gastroenterol Hepatol*. 2007;22(Suppl 1): S73-S78.

27. Ma PF, Gao CC, Yi J, et al. Cytotherapy with M1-polarized macrophages ameliorates liver fibrosis by modulating immune microenvironment in mice. *J Hepatol*. 2017;67(4):770-779.

28. Guillot A, Gasmi I, Brouillet A, et al. Interleukins-17 and 27 promote liver regeneration by sequentially inducing progenitor cell expansion and differentiation. *Hepatol Commun*. 2018;2(3):329-343.

29. Terai S, Tsuchiya A. Status of and candidates for cell therapy in liver cirrhosis: overcoming the "point of no return" in advanced liver cirrhosis. *J Gastroenterol*. 2017;52(2):129-140.

30. Shiraishi M, Shintani Y, Shintani Y, et al. Alternatively activated macrophages determine repair of the infarcted adult murine heart. *J Clin Invest*. 2016;126(6):2151-2166.

31. Duan F, Huang R, Zhang F, et al. Biphasic modulation of insulin signaling enables highly efficient hematopoietic differentiation from human pluripotent stem cells. *Stem cell research & therapy*. 2018;9(1):205.

32. Duan F, Guo L, Yang L, et al. Modeling COVID-19 with Human Pluripotent Stem Cell-Derived Cells Reveals Synergistic Effects of Anti-inflammatory Macrophages with ACE2 Inhibition Against SARS-CoV-2. *Research square*. 2020;62758.

33. Watanabe T, Niioka M, Hozawa S, et al. Gene expression of interstitial collagenase in both progressive and recovery phase of rat liver fibrosis induced by carbon tetrachloride. *J Hepatol*. 2000;33(2): 224-235.

34. Fallowfield JA, Mizuno M, Kendall TJ, et al. Scar-associated macrophages are a major source of hepatic matrix metalloproteinase-13 and facilitate the resolution of murine hepatic fibrosis. *J Immunol*. 2007;178(8):5288-5295.

35. Uchinami H, Seki E, Brenner DA, D'Armiento J. Loss of MMP 13 attenuates murine hepatic injury and fibrosis during cholestasis. *Hepatology*. 2006;44(2):420-429.

36. Iredale JP. Hepatic stellate cell behavior during resolution of liver injury. *Semin Liver Dis*. 2001;21(3):427-436.

37. Popov Y, Sverdlov DY, Bhaskar KR, et al. Macrophage-mediated phagocytosis of apoptotic cholangiocytes contributes to reversal of experimental biliary fibrosis. *Am J Physiol Gastrointest Liver Physiol*. 2010;298(3):G323-G334.

38. Bataller R, Brenner DA. Liver fibrosis. *J Clin Invest*. 2005;115(2): 209-218.

39. Triantafyllou E, Pop OT, Possamai LA, et al. MerTK expressing hepatic macrophages promote the resolution of inflammation in acute liver failure. *Gut*. 2018;67(2):333-347.

40. Dehn S, Thorp EB. Myeloid receptor CD36 is required for early phagocytosis of myocardial infarcts and induction of Nr4a1-dependent mechanisms of cardiac repair. *FASEB J*. 2018;32(1): 254-264.

41. Coelho IDN, Barros A, Macedo MP, Penha-Gonçalves C. Trem-2 promotes emergence of restorative macrophages and endothelial cells during recovery from hepatic tissue damage. *bioRxiv*. 2019.

42. Cao X, Yakala GK, van den Hil FE, Cochrane A, Mummery CL, Orlova VV. Differentiation and Functional Comparison of Monocytes and Macrophages from hiPSCs with Peripheral Blood Derivatives. *Stem Cell Reports*. 2019;12(6):1282-1297.

43. Stanley AC, Lieu ZZ, Wall AA, et al. Recycling endosome-dependent and -independent mechanisms for IL-10 secretion in LPS-activated macrophages. *J Leukoc Biol*. 2012;92(6):1227-1239.

44. Moore JK, Mackinnon AC, Wojtacha D, et al. Phenotypic and functional characterization of macrophages with therapeutic potential generated from human cirrhotic monocytes in a cohort study. *Cytotherapy*. 2015;17(11):1604-1616.

45. Haenseler W, Sansom SN, Buchrieser J, et al. A Highly Efficient Human Pluripotent Stem Cell Microglia Model Displays a Neuronal-Co-culture-Specific Expression Profile and Inflammatory Response. *Stem Cell Reports*. 2017;8(6):1727-1742.

46. Hermanson DL, Bendzick L, Pribyl L, et al. Induced Pluripotent Stem Cell-Derived Natural Killer Cells for Treatment of Ovarian Cancer. *Stem Cells*. 2016;34(1):93-101.

47. Li Y, Hermanson DL, Moriarity BS, Kaufman DS. Human iPSC-Derived Natural Killer Cells Engineered with Chimeric Antigen Receptors Enhance Anti-tumor Activity. *Cell Stem Cell*. 2018;23(2):181-92.e5.

48. Anderson JS, Bandi S, Kaufman DS, Akkina R. Derivation of normal macrophages from human embryonic stem (hES) cells for applications in HIV gene therapy. *Retrovirology*. 2006;3:24.

49. van Wilgenburg B, Browne C, Vowles J, Cowley SA. Efficient, long term production of monocyte-derived macrophages from human pluripotent stem cells under partly-defined and fully-defined conditions. *PLoS One*. 2013;8(8):e71098.

50. Kisseleva T, Cong M, Paik Y, et al. Myofibroblasts revert to an inactive phenotype during regression of liver fibrosis. *Proc Natl Acad Sci U S A*. 2012;109(24):9448-9453.

51. Liu X, Xu J, Rosenthal S, et al. Identification of Lineage-Specific Transcription Factors That Prevent Activation of Hepatic Stellate Cells and Promote Fibrosis Resolution. *Gastroenterology*. 2020;158(6): 1728-44.e14.

## SUPPORTING INFORMATION

Additional supporting information may be found in the online version of the article at the publisher's website.

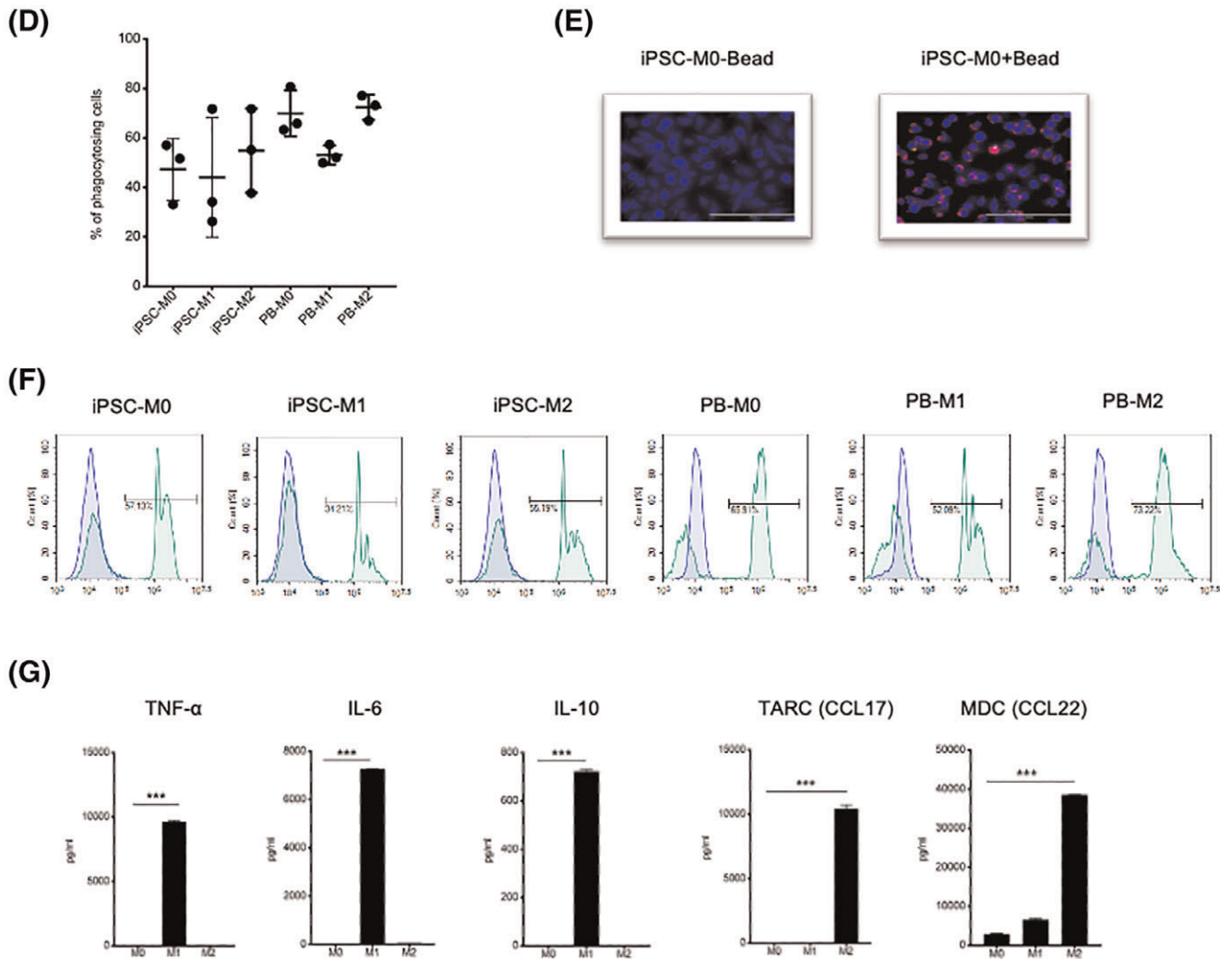| Reagent or Resource | Source | Identifier |
| --- | --- | --- |
| **Antibodies** | | |
| PE-CD34 | BD Pharmingen | Cat#: 555822 |
| APC-CD31 | Invitrogen | Cat#: 17-0319-42 |
| APC-CD43 | BD Pharmingen | Cat#: 560198 |
| APC-CD45 | BD Pharmingen | Cat#: 555485 |
| PE-CD11b | BD Pharmingen | Cat#: 557321 |
| PE-CD14 | Invitrogen | Cat#: 12-0149-42 |
| PE-CD36 | BD Pharmingen | Cat#: 550956 |
| PE-CD45 | BD Pharmingen | Cat#: 555483 |
| PE-CD68 | BD Pharmingen | Cat#: 556078 |
| PE-CD172$\alpha$ (SIRP-$\alpha$) | BioLegend | Cat#: 372103 |
| FITC-HLA-DR | BD Pharmingen | Cat#:555560 |
| PE-CD80 | BD Pharmingen | Cat#: 557227 |
| PE-CD86 | BD Pharmingen | Cat#:560957 |
| PE-CD206 | BD Pharmingen | Cat#: 555954 |
| PE-CD209 | BD Pharmingen | Cat#: 561765 |
| FITC-mouse anti-human CD68 | Bio-Rad | Cat#: MCA5709F |
| Rabbit polyclonal anti-SIRP-$\alpha$ | OriGene Technologies | Cat#: SP1202P |
| AF568-goat anti-rabbit IgG | Life Technologies | Cat#: A-11011 |
| Rabbit polyclonal anti-SMA | Abcam | Cat#: ab5694 |
| Rabbit polyclonal anti-Desmin | ThermoFisher | Cat#: Rb-9014-P0 |
| Monoclonal rat anti-F4/80 | ThermoFisher | Cat#: 14–4801-82 |
| Monoclonal mouse anti CD-68 | Abcam | Cat#: ab955 |
| HRP Horse anti-rabbit IgG (secondary) | Vector Labs | Cat#: MP-7401 |
| HRP Goat anti-rat IgG (secondary) | Vector Labs | Cat#: MP-7444 |
| Mouse on Mouse Immunodetection Kit | Vector Labs | Cat#: PK-2200 |
| **Biological Samples** | | |
| Peripheral Blood Buffy Coat | San Diego Blood Bank (https://www.sandiegobloodbank.org/) | N/A |
| **Chemicals and Recombinant Proteins** | | |
| mTeSR-1 Basal Medium | STEMCELL Technologies | Cat#: 85851 |
| mTeSR-1 5X Supplement | STEMCELL Technologies | Cat#: 85852 |
| Matrigel Matrix | Corning | Cat#: 354277 |
| STEMdiff APEL- 2 Medium | STEMCELL Technologies | Cat#: 05270 |
| X-VIVO 15-Chemically defined serum-free medium | Lonza | Cat#: 04-418Q |
| GlutaMAX™ Supplement (100X) | Gibco | Cat#: 35050079 |
| Penicillin–Streptomycin (100X) | Gibco | Cat#: 15140122 |
| 2-Mercaptoethanol (1000X) | Gibco | Cat#: 21985023 |
| Recombinant human BMP-4 | Peprotech | Cat#: 120-05 |
| Recombinant human SCF | Peprotech | Cat#: 300-07 |
| Recombinant human VEGF | Peprotech | Cat#: 100-20 |
| ROCK Inhibitor (Y-27632) | Millipore | Cat#: SCM075 |
| Recombinant human M-CSF | Peprotech | Cat#: 300-25 |
| Recombinant human IL-3 | Peprotech | Cat#: 200-03 |
| Recombinant human LPS | Sigma Aldrich | Cat#: L4391 |
| Recombinant human IFN-$\gamma$ | R&D Systems | Cat#: 285-IF-100/CF |

**Table 1** (Continued)

| Reagent or Resource | Source | Identifier |
|---|---|---|
| Recombinant human IL-4 | R&D Systems | Cat#: 204-IL-020/CF |
| Recombinant human IL-13 | R&D Systems | Cat#: 213-ILB-025/CF |
| Latex beads, carboxylate- modified polystyrene | Sigma Aldrich | Cat#: L3030 |
| DAB Substrate (HRP) | Vector Labs | Cat#: SK-4105 |
| Antigen Retrieval Solution | Agilent Dako | Cat#: S169984-2 |
| Fast-SYBR Green Master Mix | ThermoFisher | Cat#: 4385610 |
| Carbon Tetrachloride | Sigma Aldrich | Cat#: 289116 |
| **Critical Commercial Assays** | | |
| CD14-Microbeads, Human | Miltenyi Biotech | Cat#: 130050201 |
| RNeasy Mini Kit | Qiagen | Cat#: 74104 |
| iScript gDNA Clear cDNA Synthesis Kit | Bio-Rad | Cat#: 1725034 |
| Human TNF-$\alpha$ ELISA Kit | Invitrogen | Cat#: 88-7346-22 |
| Human IL-6 ELISA Kit | R&D Systems | Cat#: D6050 |
| Human IL-10 ELISA Kit | Invitrogen | Cat#: 88-7106-22 |
| TaqMan Gene CD40 | Life Technologies | ID#: Hs01002915_g1 |
| TaqMan Gene CD80 | Life Technologies | ID#: HS01045161_m1 |
| TaqMan Gene MRC1 | Life Technologies | ID#: HS00267207_m1 |
| TaqMan Gene TNF | Life Technologies | ID#: HS00174128_m1 |
| TaqMan Gene IL6 | Life Technologies | ID#: HS00985639_m1 |
| TaqMan Gene TGM2 | Life Technologies | ID#: HS00190278_m1 |
| TaqMan Gene CCL17 | Life Technologies | ID#: HS00171074_m1 |
| TaqMan Gene CCL22 | Life Technologies | ID#: HS01574247_m1 |
| TaqMan Gene GAPDH | Life Technologies | ID#: HS02758991_g1 |
| **Experimental Models: Cell Lines and Organisms/Strains** | | |
| Human: iPS Cells | Dan S. Kaufman Laboratory | N/A |
| Human: Peripheral Blood Monocytes | Dan S. Kaufman Laboratory | N/A |
| Murine: Rag2$^{-/-}$ gamma c$^{-/-}$ | Tatiana Kisseleva Laboratory | N/A |
| **Software and Algorithms** | | |
| FlowJo | https://www.flowjo.com/ | N/A |
| NovoExpress | https://www.aceabio.com/novoexpress | N/A |
| Infinite® 200 PRO Plate Reader | Tecan Group Ltd. | N/A |
| CFX Manager Software | BioRad | N/A |
| Prism version8 | Prism Graphpad | N/A |
| IncuCyte real-time image system | Essen Bioscience | N/A |
| ImageJ | https://imagej.net/Welcome | |

**Figure 1    Production of human iPSC-derived Macrophages.** A, B) Schematic diagram showing culture conditions required for each differentiation step from human iPSCs to generation of polarized macrophages. Briefly, to produce hematopoietic progenitor cells from human iPSCs, spin EBs are formed after plating ~8000 human iPSCs per well of a round-bottom 96-well plate in a differentiation medium containing the stem cell factor (SCF), vascular endothelial growth factor (VEGF) and bone morphogenic protein 4 (BMP4). After 6 days of culture, EBs transferred to 6-well plates in media supplemented with M-CSF and IL-3. After about 1–2 weeks, the EBs produce human macrophage progenitor cells (iPSC-MPro). Next, human iPSC-MPro are transferred to new plates in serum-free media containing M-CSF and allow to mature for 5-7 days (iPSC-M0). Macrophage can then be primed in vitro to either M1 or M2 phenotypes by treating with LPS + IFN-g or IL-4 + IL-13, respectively. Representative images of each differentiation step including modified Giemsa stain of human iPSC-M0, M1 and M2 are depicted (scale; 100 μm). C) Flow cytometric analysis of human iPSCs (TRA-1-81 and SSEA-4) and D) Hematopoietic progenitor cells (EBs; CD34, CD31, CD43 and CD45). E) Cumulative number of human iPSC-MPro generated in this system demonstrates we can continuously produce human iPSC-MPro from undifferentiated human iPSCs for more than 12 weeks at a quantity of ~1 x $10^6$ cells/week/well (6-well plate). F) Phenotypic characterization of human iPSC-MPro over different harvests is shown
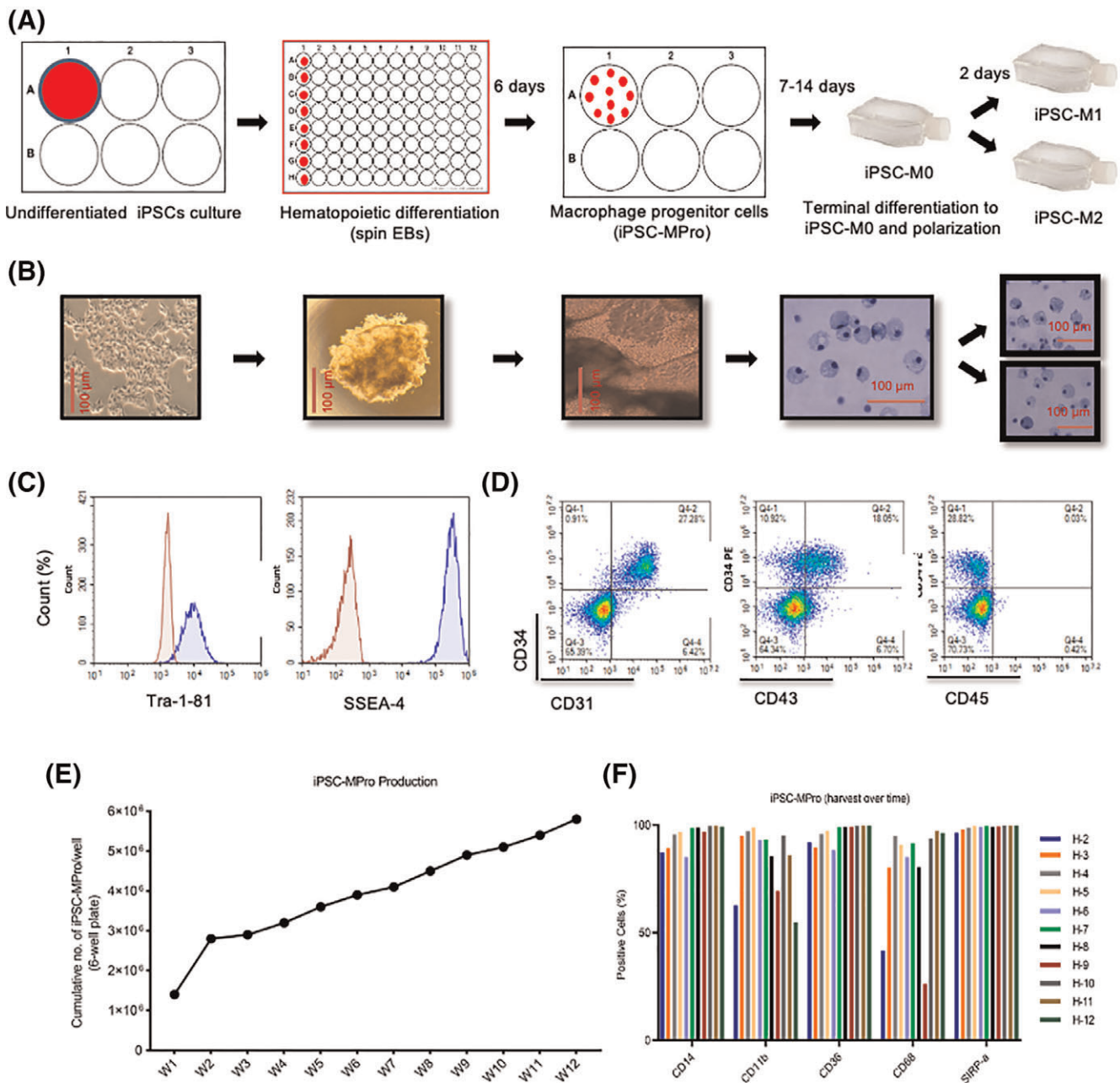
**Figure 2** **Characterization of human iPSCs-derived Macrophages.** A) Flow cytometric analysis demonstrate expression of typical antigenic markers CD14, CD11b, CD68, CD86, HLA-DR and SIRP-α on human iPSC-M0 and human PB-M0 indicating that human iPSC-M0 have the same phenotype to that of human PB-M0. B) Flow cytometric analysis of expression of typical M1/M2 macrophage surface markers; CD80 and CD206 respectively in human iPSC and PB-derived macrophages. C) RT-qPCR for M1 (CD80, CD40) and M2-associated genes (CD206, TGM2) in human iPSC and PB-derived macrophages (M0, M1 and M2). Data represent the mean +/− SEM of n = 3 technical replicates. Statistical analysis was performed using one-way ANOVA with multiple comparisons. D) Phagocytosis of carboxylate-modified polystyrene-labeled latex beads (2 hours incubation) is used to demonstrate function of human iPSC and PB-derived macrophages (M0, M1 and M2) as analyzed by flow cytometry (blue filled: cells treated with 2 μm beads; red filled: untreated cell). E) Representative image of fluorescent microscopy of human iPSC-M0 without and with latex beads, respectively is shown (scale; 200 μm). F) Representative histograms of bead phagocytosis of human iPSC and PB-derived macrophages (M0, M1 and M2). G) MSD analysis of cytokine expression (TNF-a, IL-6, IL-10, TARC, MDC) in human iPSC-derived macrophages (M0, M1 and M2). Data represent the mean +/− SEM of n = 2 biological replicates. Statistical analysis was performed using one-way ANOVA with multiple comparisons

**(D)**



**(E)**

iPSC-M0-Bead          iPSC-M0+Bead



**(F)**

iPSC-M0    iPSC-M1    iPSC-M2    PB-M0    PB-M1    PB-M2



**(G)**

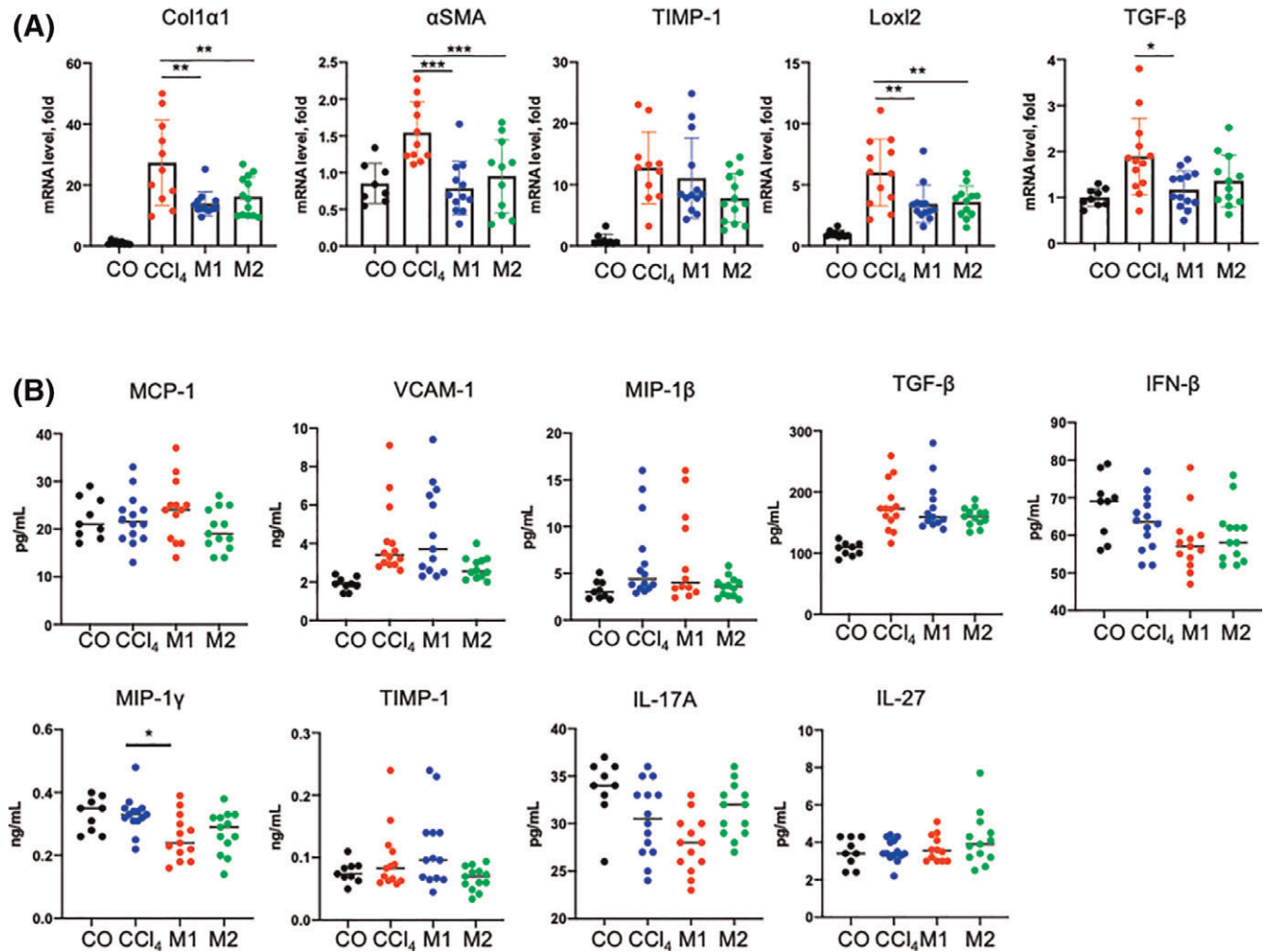TNF-α    IL-6    IL-10    TARC (CCL17)    MDC (CCL22)

**Figure 3** **Gene expression analysis of different human iPSC-derived macrophages.** A) Heatmap analysis of differentially expressed known genes of M1 and M2 macrophages in human iPSC-M1 and human iPSC-M2 and B) a select list of previously reported genes involved in tissue repair and regeneration shown in human iPSC-M1 and human iPSC-M2 via RNA sequencing (N = 3 biological replicates)
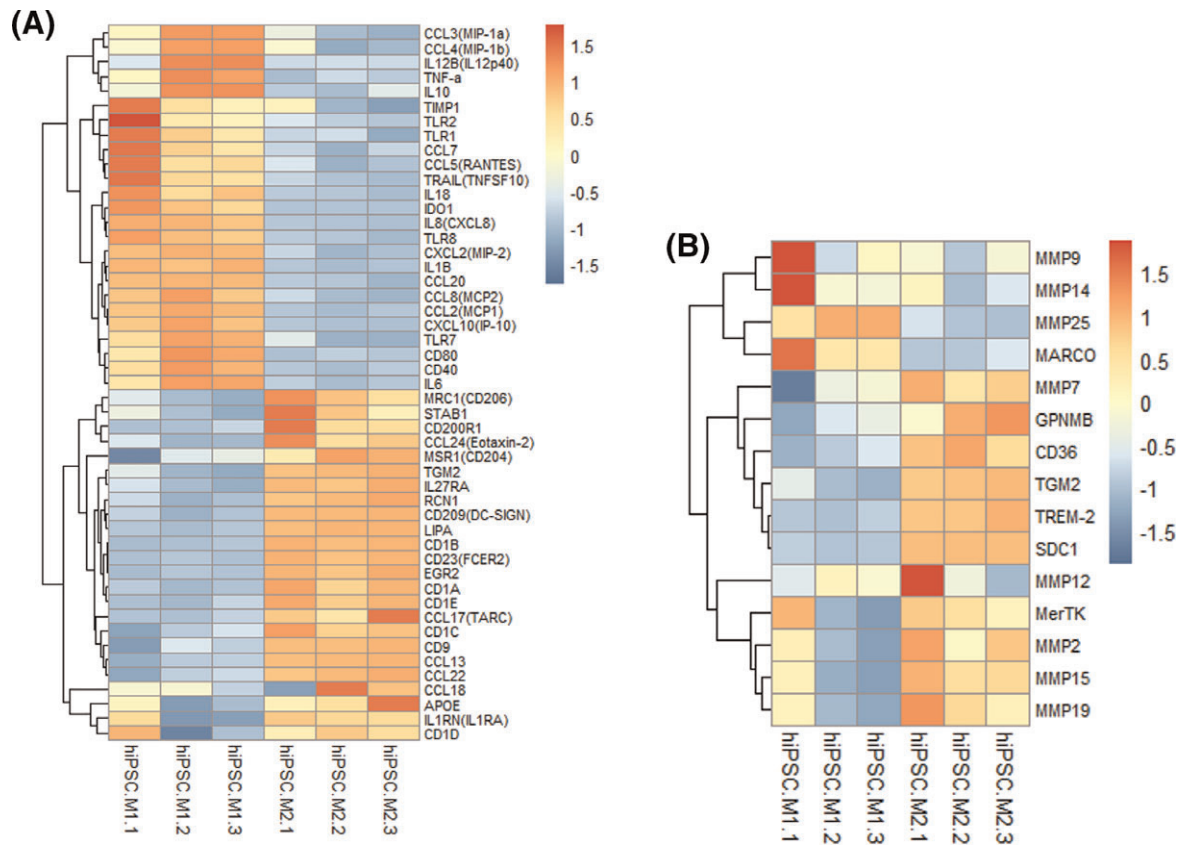
**Figure 4** **Analysis of in vivo efficacy of human iPSC-derived macrophage populations in rag2$^{-/-}$ gc$^{-/-}$ mice.** A) Timeline of *in vivo* fibrosis induction and therapeutic administration of human iPSC-M1 and iPSC-M2 macrophages. 4 groups of rag2$^{-/-}$ gc$^{-/-}$ mice received: corn oil only (CO) (n = 9), CCL$_4$ only (n = 14), CCL$_4$ + human iPSC-M1 (n = 13) or CCL$_4$ + human iPSC-M2 (n = 13). B) Liver weight to body weight ratio. Ratio was significantly lower in human iPSC-M2 treated livers compared to both CCl$_4$ and human iPSC-M1 ($P$ = 0.02, 0.004, respectively). C) Gross morphology of liver from different groups of mice. D) Mouse livers were stained for H&E, Sirius Red, aSMA, Desmin, and F4/80. Average positive area was calculated as a percentage for all mice in each group; only representative images are shown (x4 objective). D) Quantification of staining for each marker is shown below the fields (*$P$ < 0.05, **$P$ < 0.01, ***$P$ < 0.001)
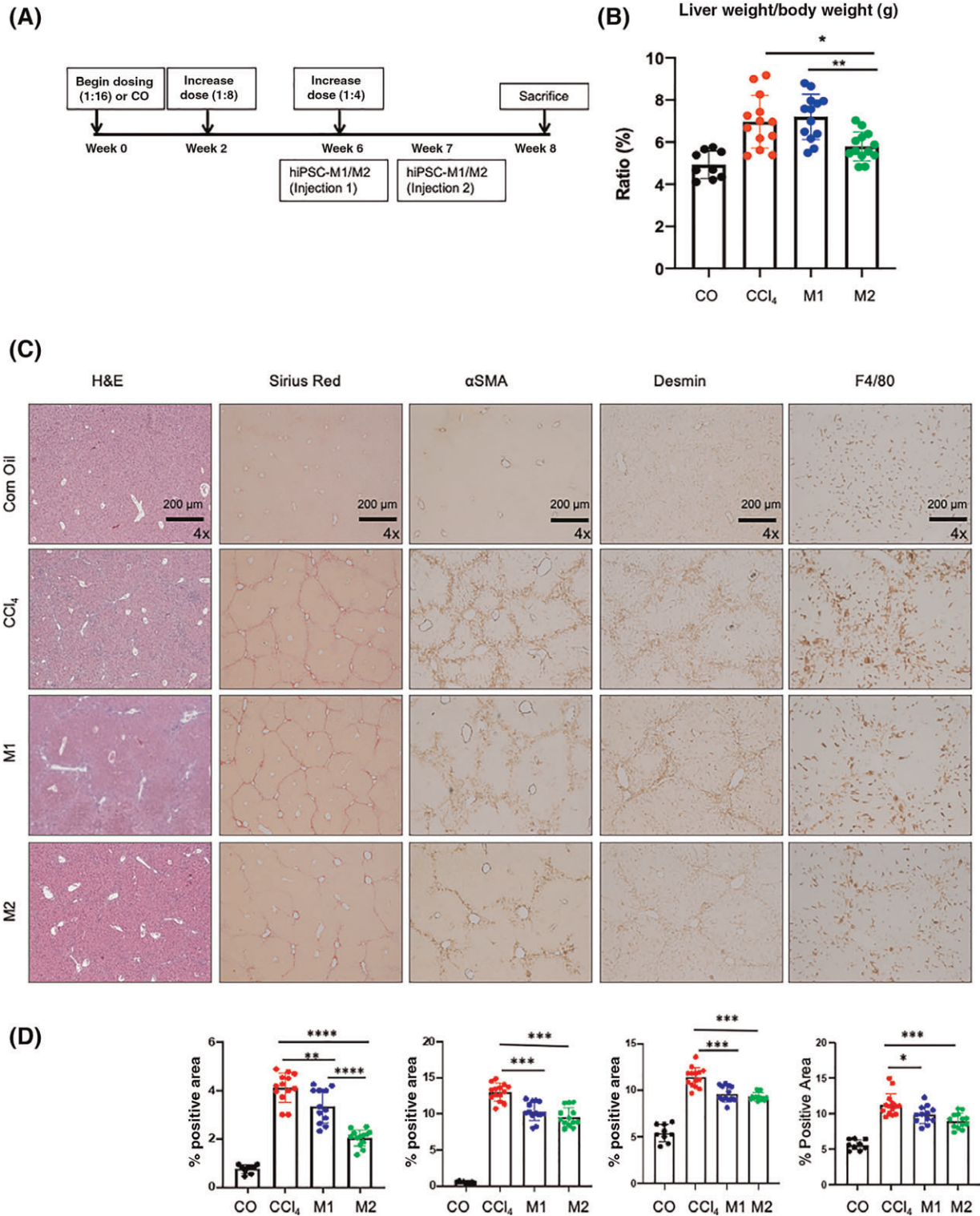
**Figure 5** Gene and cytokine expression analysis in liver of rag2$^{-/-}$ gc$^{-/-}$ mice treated with iPSC-derived macrophage populations. A) Quantitative RT-PCR analysis for select markers of fibrosis. A one-way analysis of variance was used to compare all samples (*$P < 0.05$, **$P < 0.01$, ***$P < 0.001$). Data are shown as fold change compared with corn oil treated controls. B) Analysis of a panel of cytokines/chemokines on liver homogenates performed by Ampersand Biosciences. A one-way analysis of variance was used to compare all samples (*$P < 0.05$, **$P < 0.01$, ***$P < 0.001$)

# Human Induced Pluripotent Stem Cell-Derived Macrophages Ameliorate Liver Fibrosis

Somayeh Pouyanfard[1]  |  Nairika Meshgin[2]  |  Luisjesus S Cruz[1]  |  Karin Diggle[2]  |  Hamidreza Hashemi[3]  |  Timothy V Pham[4]  |  Manuel Fierro[1]  |  Pablo Tamayo[4]  |  Andrea Fanjul[5]  |  Tatiana Kisseleva[2]  |  Dan S Kaufman[1] ⓘ

[1]Department of Medicine, University of California, La Jolla, California, USA

[2]Department of Surgery, University of California San Diego, La Jolla, California, USA

[3]Immunity and Pathogenesis Program, Sanford Burnham Prebys Medical Discovery Institute, La Jolla, California

[4]Moores Cancer Center and Department of Medicine, University of California San Diego, La Jolla, California, USA

[5]Gastroenterology Drug Discovery Unit, Takeda Pharmaceutical Company Limited, San Diego, California, USA

**Correspondence**
Dan S. Kaufman; Department of Medicine, University of California, San Diego, La Jolla, California, USA; Phone number +1-858-822-1777;
Email: dskaufman@ucsd.edu

**Graphical Abstract**

The contents of this page will be used as part of the graphical abstract of html only. It will not be published as part of main.
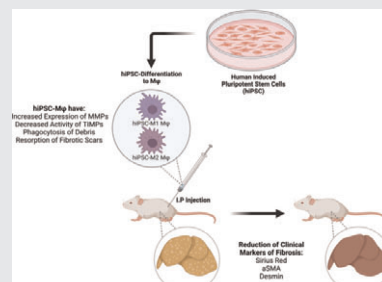


Human iPSCs are efficiently differentiated into both M1 and M2 macrophages. These cells were used to treat liver fibrosis in an immunodeficient mouse model. This treatment led to improvement in the fibrosis as measured by several complementary assays.